Acta metall. Vol. 37, No. 10, pp. 2659–2671, 1989
Printed in Great Britain

0001-6160/89 $3.00 + 0.00
Pergamon Press plc

ROLE OF INTERFACIAL GRAIN-BRIDGING SLIDING FRICTION IN THE CRACK-RESISTANCE AND STRENGTH PROPERTIES OF NONTRANSFORMING CERAMICS

S. J. BENNISON† and B. R. LAWN

Ceramics Division, National Institute of Standards and Technology, Gaithersburg, MD 20899, U.S.A.

(*Received* 10 *November* 1988; *in revised form* 15 *March* 1989)

Abstract—A grain-bridging model of crack-resistance or toughness (R-curve, or T-curve) properties of nontransforming ceramics is developed. A key new feature of the fracture mechanics treatment is the inclusion of internal residual (thermal expansion mismatch) stresses in the constitutive stress-separation relation for pullout of interlocking grains from an embedding matrix. These internal stresses play a controlling role in the toughness properties by determining the scale of frictional tractions at the sliding grain–matrix interface. By providing a physical account of the underlying micromechanics of the bridging process the analysis allows for predetermination of the material factors in the constitutive relation, thereby reducing parametric adjustments necessary in fitting the theoretical toughness curve to experimental data. The applicability of the model is illustrated in a case study on indentation-strength data for a "reference" polycrystalline alumina with particularly strong T-curve characteristics. From theoretical fits to these data the constitutive relation, and thence the entire T-curve, can be deconvoluted. This "parametric calibration", apart from demonstrating the plausibility of the model, allows for quantitative predictions as to how the toughness and strength characteristics of ceramics depend on such microstructural variables as grain size and shape, grain boundary energy, level of internal stress and sliding friction coefficient. An indication of this predictive capacity is provided by a preliminary calculation of the grain-size dependence of strength, using some existing data for other aluminas as a basis for comparison.

Résumé—Nous développons un modèle, par liaison des grains, des propriétés de résistance aux fissures ou de dureté (courbe R ou courbe T) dans des céramiques stables. Une caractéristique nouvelle essentielle du traitement de la mécanique de la rupture consiste à inclure les contraintes résiduelles internes (désaccord de dilatation thermique) dans la relation de base contrainte-rupture pour l'arrachement de grains imbriqués hors de la matrice qui les entoure. Ces contraintes internes contrôlent les propriétés de dureté en déterminant l'échelle des tensions de frottement aux interfaces matrice/grain qui glissent. Parce qu'elle fournit une description physique des micromécanismes sous-jacents du processus de liaison, cette analyse permet de déterminer à l'avance les facteurs de matériau dans la relation de base, et donc de réduire les ajustements de paramètres nécessaires pour faire coïncider les courbes théoriques de dureté et les résultats expérimentaux. L'applicabilité du modèle est illustrée dans une étude des valeurs expérimentales de la résistance à l'indentation d'une alumine polycristalline "de référence" dont les caractéristiques de la courbe T sont particulièrement élevées. Quand on ajuste la théorie à ces résultats, on peut déconvoluer la relation de base et donc la courbe T entière. Cet "étalonnage paramétrique", outre qu'il démontre la vraisemblance de notre modèle, permet de prévoir de façon quantitative comment les caractéristiques de résistance et de dureté des céramiques dépendent de variables microstructurales telles que la taille et la forme des grains, l'énergie intergranulaire, le niveau de la contrainte interne et le coefficient de frottement en glissement. Un calcul préliminaire de l'effect de la taille de grains sur la résistance, utilisant comme base de comparaison quelques résultats disponibles pour des alumines différentes, fournit une indication de cette aptitude à prévoir.

Zusammenfassung—Ein Körner überbrückendes Modell des Rißwiderstandes oder der Zähigkeit (R-Kurve oder T-Kurve) wird für sich nicht umwandelnde Keramiken entwickelt. Als wichtiger neuer Ansatz in der bruchmechanischen Behandlung werden innere Restspannungen (hervorgerufen durch thermische Fehlpassungen) in die grundlegende Beziehung zwischen Spannung und Weg für das Herausziehen miteinander verhakter Körner aus der umgebenden Matrix aufgenommen. Diese inneren Spannungen kontrollieren die Zähigkeitseigenschaften, indem sie den Rahmen der Reibung an der gleitenden Korn-Matrix-Grenzfläche bestimmen. Mit der physikalischen Beschreibung der Mikromechanik des Überbrückungsprozesses können die Materialfaktoren in der Grundbeziehung vorher bestimmt werden, wobei die Anpassung der theoretischen Zähigkeitskurve an die experimentellen Ergebnisse mit Parameter vereinfacht wird. Die Anwendbarkeit des Modelles wird mit einer Untersuchung der Festigkeit bei Stempeleindruck von einem polykristallinen "Referenz"-Aluminiumoxid mit besonders starker T-Kurven-Charakteristik gezeigt. Aus der theoretischen Anpassung an diese Daten kann die Grundbeziehung und damit die gesamte T-Kurve aus einer Dekonvolution erhalten werden. Diese "parametrische Eichung" ermöglicht, neben der Demonstration der Plausibilität des Modelles, die quantitativen Aussagen, wie Zähigkeits- und Festigkeits-eigenschaften von Keramiken von mikrostrukturellen Variablen wie Korn-

†Guest Scientist: on leave from the Department of Materials Science and Engineering, Lehigh University, Bethlehem, PA 18015, U.S.A.

größe und-form, Korngrenzenergie, Niveau der inneren Spannungen und Koeffizient der Gleitreibung abhängen. Ein Hinweis auf diese Fähigkeit der Voraussage wird geliefert, indem die Abhängigkeit der Festigkeit von der Korngröße berechnet wird, wobei einige verfügbare Daten für andere Aluminiumoxide als Grundlage für einen Vergleich herangezogen werden.

1. INTRODUCTION

Much recent attention has been paid to the phenomenon of a systematically increasing fracture resistance with crack extension in ceramics (R-curve, or T-curve). In nontransforming ceramics† the *magnitude* of this increase can be respectable, i.e. in excess of a factor of three, depending on the microstructure [1–12]. The *range* of extension over which the increase can occur is perhaps even more impressive, amounting in some instances to some hundreds of grain dimensions. The R-curve has a stabilising influence on crack growth, strikingly manifested in strength properties as a tendency to flaw insensitivity [13]: hence "flaw tolerance", a concept with especially strong appeal to those concerned with structural design.

This flaw tolerance is especially well demonstrated in indentation-strength tests [3, 4, 9], where Vickers indentations are used to introduce controlled starter flaws into the surfaces of strength specimens. At decreasing indentation load the strength deviates away from the (logarithmic $-1/3$) dependence of strength on indentation load predicted for materials with single-valued toughness, and tends instead toward a well-defined plateau. Such plateaus have been reported in a wide range of ceramic materials [3, 9], indicating a certain generality in the R-curve phenomenology. Moreover, these plateaus, where they are pronounced, tend to the strengths for failures from processing defects. Thus the indentation-strength test provides R-curve information in the crack-size domain most pertinent to designers, i.e. the domain of natural flaws.

There is now a weight of direct evidence demonstrating that the principal mechanism of rising crack resistance behaviour in nontransforming ceramics is grain-localised *bridging* at the crack interface *behind* the advancing tip [4, 5, 7, 10]. In particular, it is observed that frictional tractions associated with the pullout of interlocking grains can restrain the crack opening for large distances (up to several mm in some aluminas) behind the tip, thereby accounting for the range of the R-curve. A traditional preoccupation of ceramics fracture analysts with post-mortem fractographic observations had long precluded identification of this mechanism: the very act of failure destroys the bridges. It is only recently, as a result of *in situ* crack extension observations made *during* the stressing to failure, that the bridging mechanism has become clear. Again, the mechanism appears to be common to a wide range of ceramics, especially noncubic ceramics that fail by intergranular failure.

Theoretical descriptions of the bridging mechanism are in their infancy. Mai and Lawn [13] presented a model based on a distribution of closure tractions across the crack walls. This distribution gives rise to a "microstructural" stress intensity factor, which augments the stress intensity factor associated with the applied loading. Since this microstructural stress intensity factor is negative it can be regarded as part of the toughness/crack-size function, $T(c)$; thence the R-curve (or, more strictly, T-curve). Key to the theoretical development is the specification of a constitutive stress-separation function defining the physical restraint exerted by individual bridges. In this regard the approach of Mai and Lawn was phenomenological; they recognised the need for an extensive functional "tail" to account for the large traction zone behind the crack tip, but adopted an empirical inverse relation to describe it. Their empirical function contains the necessary ingredients for a macroscopic description of the failure mechanics, allowing for, among other things, a deconvolution of indentation-strength data to obtain the T-curve [9]. However, while there is some precedent in the concrete literature for tail-dominated relations [14], the empirical approach precludes a fundamental understanding of the underlying material aspects of the phenomenon. What elements of the microstructure control the restraining tractions, and how might we adjust these elements to optimise the R-curve characteristics?

In this paper we set out to answer such questions by incorporating a stress-separation function based on a specific physical mechanism of grain pullout for noncubic materials. We consider the bridging grains to be "locked" into the "matrix" on either side of the crack interface by *internal thermal expansion mismatch stress*. The resistance to pullout then derives primarily from *Coulomb friction at the sliding matrix–grain interface*. In this sense the mechanism is analogous to that of fibre pullout in ceramic composites. Indeed, we shall borrow from established fracture mechanics descriptions for composites in our own formulations. We are led to consider internal stresses as an important factor for two reasons: first, because of an apparent diminishing of the T-curve behaviour with addition of intergranular phases in alumina ceramics, the second phase presumably acting to relax the stress buildup during the processing [3, 4]: second, because the T-curve effect has been observed in noncubic, but not cubic, ferroelectric ceramics (viz. barium titanate below and above the Curie temperature [3]). We emphasise at the outset that these internal stresses enter the T-curve analysis

†As distinct from *transforming* ceramics (zirconia). The significant increases in toughening in this latter class of material are relatively well documented and understood.

only via their influence on the micromechanics of bridging and not via any direct interaction with the field of the advancing tip; we shall argue that the latter possibility, considered as a potential source of toughness variation in the earlier literature [15], cannot account for the scale of the T-curve observed in the materials to be investigated here.

Our goal is to formulate a theory for quantifying the role of such microstructural parameters as size, shape and spacing of bridging grains, grain boundary energy and intergranular sliding friction coefficient, on the strength properties of ceramics. To illustrate the formalism we fit our toughness equations to some data from previous indentation–strength tests on an alumina with particularly strong T-curve characteristics. With the results of this fit we then make some preliminary predictions of the strength/grain-size dependence. The ultimate hope is that such an approach might be used to establish a theoretical base for a processing strategy that allows for optimisation of strength properties of ceramics for specific applications.

2. MICROMECHANICS OF FORCE–SEPARATION FUNCTION FOR INTERLOCKING GRAINS WITH INTERNAL-STRESS-MODIFIED FRICTIONAL TRACTIONS

2.1. Geometrical factors and internal stresses

An important element of our model is the geometrical configuration of interlocking grains at the crack interface, and the role of local residual internal stresses in determining subsequent frictional restraints as these grains are progressively disengaged from the crack walls. Such stresses were first discussed in the context of grain bridging by Swain [16]. However, Swain confined his attention to estimates of the spatial extent of the T-curve, without any consideration of the shape or height of this curve.

Consider first thermal expansion mismatch stresses normal to the separation plane along which the crack is to propagate. These internal stresses arise from crystallographic anisotropy of individual grains within the material microstructure. They are *conservative*, in that they may be relaxed and restored in any elastic operation that displaces the opposing half-spaces across the separation plane. They consist of both tensile stresses, σ_R, and compressive stresses, $\sigma_{\bar{R}}$

$$\sigma_R = +\beta_+ E\Delta\alpha\Delta T \tag{1a}$$

$$\sigma_{\bar{R}} = -\beta_- E\Delta\alpha\Delta T \tag{1b}$$

where E is Young's modulus, $\Delta\alpha$ is the differential thermal expansion coefficient, ΔT is the temperature range through which the material deforms elastically, and the β are coefficients <1. Those grains subject to compression will tend to remain in contact with both sides of the interface in any such reversible separation process, and thence constitute incipient "bridges"; those remaining grains subject to tension may then be considered as making up the constitutive "matrix".

Now define a characteristic grain size l and characteristic bridge spacing d, as illustrated schematically in Fig. 1(a) for a periodic rectangular lattice, such that the area fraction of bridges is $l^2/2d^2$. Then the requirement for the tensile and compressive stresses to balance over any potential separation plane is that

$$\sigma_R(1 - l^2/2d^2) = -\sigma_{\bar{R}}(l^2/2d^2). \tag{2}$$

For the ideal case of a unimodal, homogeneous grain structure, where we expect equal probability of tensile and compressive stress, i.e. $\beta_+ = \beta_-$, equation (2) requires that $d = l$. This corresponds to the limiting configuration in which every alternate grain is (on average) a bridge.

How might these internal stresses exert restraining forces on prospective crack walls? When we deal with fracture mechanics later we will need to distinguish certain crack-size domains. For very small cracks in the initial stages of development, $c < d$, the walls will feel the full influence of either the matrix tensile stress σ_R (or, alternatively, the compressive stress $\sigma_{\bar{R}}$ in the relatively unlikely event of cracks generating from within the bridges themselves). Thus in this domain the discreteness of the microstructure is crucial. For very large cracks, $c \gg d$, the internal stresses must average out to zero over the potential separation plane. In the intermediate domain within the first few bridge intersections the microstructural discreteness, representable as alternate areas of positively and negatively stressed grain facets, will rapidly wash out (the crack area increasing with $\approx c^2$ for the penny-like geometry). Accordingly, we make the approximation that the net internal elastic stress across any crack area beyond the first bridge is zero.

If this last approximation holds, then the origin of the closure stresses needed to produce toughening

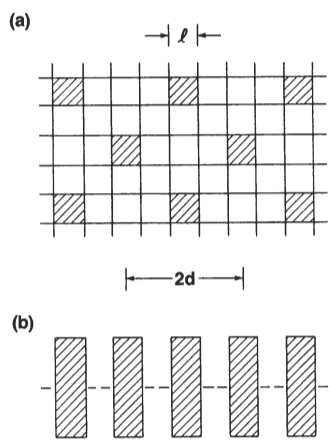

Fig. 1. Schematic geometry of bridged interface, in rectangular "lattice" representation of microstructure: (a) projection normal to crack plane; (b) profile view along crack plane. Shaded areas denote bridging grains. Characteristic dimensions l, grain size, d, bridge spacing. (The factor 2 in our definition of the bridge separation is so that later in Fig. 4 we may conveniently delineate the region between no-bridging and bridging simply by $c = d$.)

must lie in some subsidiary, *nonconservative* source. Suppose the fracture to be intergranular, and consider the internal stresses *transverse* to the separation plane at the grain–matrix interfaces [Fig. 1(b)]. Some of the grains (those destined to act as bridges) will be in a state of residual compression. At this stage we make no attempt to distinguish fine details of the stress state, assuming a uniform distribution σ_R^- at the boundaries. We shall propose below that Coulomb sliding friction at the compressive grain–matrix interface provides the dominant closure stress as the surfaces are separated along the grain boundaries. It is possible that not all compressively stressed grains will be ideally oriented to provide effective interlocking, in which case we may generally expect $d > l$, even in ostensibly homogeneous microstructures. In this model the internal stresses, although not the direct cause of the closure, are (contrary to what one might at first sight conclude from the preceding paragraph) far from benign, since they determine the magnitude of the frictional tractions.

Accordingly, we need to determine a constitutive relation betwen closure stress, p, and (half) crack-wall separation, u, for this dissipative friction component. We shall adopt the convention, consistent with our notion that frictional tractions will always act to oppose crack opening, that *positive* $p(u)$ denotes *closure*. The function $p(u)$ is derived for different crack-size regions in the following subsections.

2.2. Frictional debonding at matrix–grain interface

Suppose the crack intersects a grain in residual compression, Fig. 2(a). The intersected grain initially exerts an opening force on the crack walls. As separation behind the advancing crack tip proceeds, this opening force diminishes and ultimately becomes negative (closure), leaving the grain embedded in the matrix on both sides of the interface. This is the first stage of bridge formation. The ensuing build-up of differential strain between the grain and matrix results in interfacial debonding, starting at the crack plane and extending stably up the interface. Simultaneous with this debonding is the onset of resistive, frictional tractions, increasing in intensity until debonding is effectively complete.

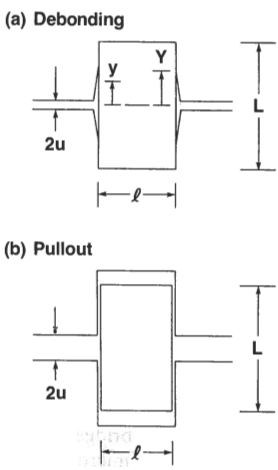

Fig. 2. Stages of friction grain detachment from matrix at separating interface. (a) Initial debonding stage, with progression of shear crack up the grain-matrix walls to $2y = 2Y$ at separation $2u$. (b) Subsequent sliding pullout to disengagement at $2u = 2u_*$. Long grain dimension L is limiting value that $2Y$ or $2u_*$ may attain.

Calculations of the debonding process have been carried out in the ceramic composites literature, particularly in the context of fibre-reinforced composites. We resort to one such calculation, by Marshall and Evans [17], deferring details to the Appendix. At the outset we may assert that the debonding is unlikely to make a profound contribution to the energy dissipation; although frictional forces are involved, the distances over which these forces are active is limited to the relatively small elastic displacements within the internally stressed bridges. Balancing the integrated frictional shear lag stress over the debonded interface area against the axial stress in the residually stressed bridging grain, one obtains a square root dependence of closure stress p on u [17] (Appendix)

$$p(u) = \{(2\mu\sigma_R E\lambda/l^2)^{1/2}/(2d^2/l^2 - 1)\}\, u^{1/2} - \sigma_R \quad (3)$$

where λ is the circumferential distance around the debonding grain at the separating interface (e.g. $\lambda = 4l$ for the rectangular geometry in Fig. 1) and μ is the friction coefficient. We note the appearance of E in equation (3), consistent with an elastic relaxation process. We note also the negative intercept, $p(0) = -\sigma_R$, indicative of the *opening* stress that pertains at initial wall separation.

2.3. Sliding friction grain pullout

Once debonded, the grain can slide out of the matrix, Fig. 2(b). The frictional closure stress on the crack wall is now exerted by individual bridging grains as they are pulled out of the embedding matrix. The force exerted by one grain at any wall–wall separation $2u$ is given by the product of: $\lambda(2u_* - 2u)$, with $2u_*$ the separation at which the grain disengages (area of grain wall in contact with matrix); μ (sliding friction coefficient); and $-\sigma_R^-$ (normal, clamping stress). Noting that the average area occupied by one bridge is $2d^2$ and recalling equations (1) and (2), we obtain

$$p(u) = (\mu\sigma_R\lambda u_*/d^2)(2d^2/l^2 - 1)(1 - u/u_*). \quad (4)$$

This relation has the same characteristic falloff with u as assumed empirically in earlier studies [8, 9], except that here it is explicitly linear. Such a linear dependence is contingent on an invariant cross-sectional grain geometry during pullout [18], as implicit in our consideration of a rectangular microstructure in Fig. 2. The representation in Fig. 2 also depicts the frictional forces as distributed uniformly and symmetrically over the entire matrix/bridging–grain remnant "contact" interface.

Direct observations of the bridging configurations indicate that the reality is more complex: the bridging configuration is, in general, far from rectangular, and the frictional contact regions tend to be concentrated at points of geometrical irregularity (ledges, re-entrant corners, etc.), often across a single (compressively stressed) facet of the disengaging grain, where the resistance forces can be intense (see, for instance, Fig. 12 of Ref. [7]). Ours is a somewhat idealised representation of the closure stress function. Nevertheless, equation (4) does contain the essential physics of the proposed separation process, and is well structured for incorporation of critical microstructural parameters.

In deriving equation (4) we have not considered the possibility that the bridging grains might rupture transgranularly. If such rupture *were* to occur, $p(u)$ would cut off prematurely at some critical separation. Such cutoffs are indeed predicted in ceramic composites with continuous fibres [17]. They might be expected in our monophase ceramics if the frictional stresses were allowed to build up sufficiently, e.g. at large grain sizes. For the present we neglect this possibility.

Because sliding friction can occur over a large fraction of the embedded grain dimension, we may anticipate pullout to dominate debonding as a contributory factor in the toughening.

2.4. Composite p(u) function

Now let us combine the results in Sections 2.3 and 2.4 to obtain a composite closure stress–separation function $p(u)$ for the entire evolution of the bridge, from initial formation to rupture and beyond. It is re-emphasised that we are dealing with an approximation in which a discrete distribution of bridging forces is replaced by a continuous stress function. We recall that this approximation is good only for cracks with area large compared to the area occupied by a single bridge ($c \gg d$). As alluded in Section 2.1, we shall extend the formalism down to the intermediate crack-size domain, but not to the small-crack domain ($c < d$) where the internal stresses dominate.

Notwithstanding these provisos, we reduce the closure stress function as follows

$$p(u) = p_D(u/u_*)^{1/2} - \sigma_R \quad (0 \leqslant u \leqslant u_+) \tag{5a}$$

$$p(u) = p_M(1 - u/u_*) \quad (u_+ \leqslant u \leqslant u_*) \tag{5b}$$

$$p(u) = 0 \quad (u \geqslant u_*) \tag{5c}$$

where the scaling quantities

$$p_D = (2\mu\sigma_R E\lambda u_*/l^2)^{1/2}/(2d^2/l^2 - 1) \tag{6a}$$

$$p_M = (\mu\sigma_R \lambda u_*/d^2)(2d^2/l^2 - 1) \tag{6b}$$

are respectively the shear-lag stress in equation (3) evaluated at $u = u_*$ in the absence of residual stress σ_R and the sliding friction stress in equation (4) evaluated at $u = 0$. Equation (5) is plotted schematically in Fig. 3. Thus we have a function $p(u)$ with negative

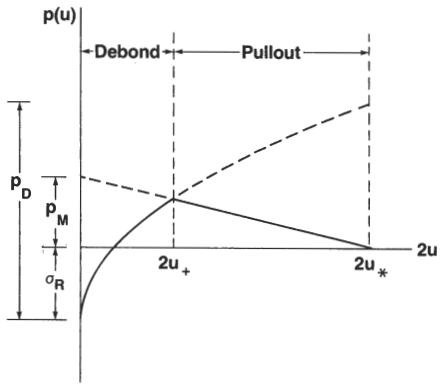

Fig. 3. Schematic plot of $p(u)$ closure function, equation (5). Area under the composite solid curve is a measure of the energy absorbed by the debonding-pullout bridging process.

intercept at $p(0) = -\sigma_R$, square root dependence to the crossover point at $u = u_+$, and linear decline to $p(u_*) = 0$. The area under the curve in Fig. 3 represents the energy of separation of the bridged interface.

It is instructive to determine the crossover point where the $p(u)$ functions in equations 5(a) and (b) are identically equal

$$u_+/u_* = (p_D/2p_M)^2 \times \{[1 + 4p_M(p_M + \sigma_R)/p_D^2]^{1/2} - 1\}^2. \tag{7}$$

As indicated above, we may generally expect to find $p_D \gg p_M + \sigma_R$, $u_+/u_* \simeq [(p_M + \sigma_R)/p_D]^2 \ll 1$, in which event the debonding term will be relatively insignificant in the fracture mechanics. We shall find this to be the case for our alumina later (Section 4).

3. FRACTURE MECHANICS

3.1. General equilibrium requirements

Begin by defining a *general* stress intensity factor condition for the equilibrium of a crack subject to an applied tensile loading field (K_a), a flaw-localised internal tensile field associated with any residual nucleation forces on the crack (K_r) [19], and a microstructure-associated closure field (K_μ) [8]. These stress intensity fields are linearly superposable. A stationary value obtains when the net K on the crack tip, $K_*(c)$ say, just balances the toughness associated with reversible creation of surfaces, T_0

$$K_*(c) = K_a(c) + K_r(c) + K_\mu(c) = T_0 = (2\gamma_0 E')^{1/2} \tag{8}$$

with $E' = E/(1 - \nu^2)$ for plane strain, ν Poisson's ratio. Here γ_0 is an appropriate surface energy term. For the case of special interest to us, that of intergranular fracture, we have

$$2\gamma_0 = 2\gamma_s - \gamma_B \tag{9}$$

with γ_s the surface energy of the bulk solid and γ_B the grain boundary formation energy.

It is convenient to restate the above equilibrium requirement in a form appropriate to the R-curve phenomenology. We note that, like K_a, K_r is a truly extrinsic mechanical *driving* force on the crack system. (We shall identify K_r specifically for identation cracks below.) The quantity K_μ on the other hand is an intrinsic *resistive* term, always negative, so is more appropriately regarded as part of the toughness, i.e. $T_\mu = -K_\mu$. Accordingly

$$K_A(c) = K_a(c) + K_r(c)$$
$$= T_0 + T_\mu(c) = T(c). \quad (10)$$

The composite, crack-size dependent toughness term T is equivalent to the quantity K_R used by some: we adopt the T notation to avoid potential confusion with the negative sign in K_μ, and to emphasise that we are considering an intrinsic material property rather than an extrinsic mechanical force. We may note the equivalence of the above stress intensity factor relation $K_c = K_A = T$ with the mechanical release rate relation $G_c = R$, via the familiar connection $T = (RE')^{1/2}$ [13]; hence our use of the term "T-curve" instead of the more familiar "R-curve".

The critical condition for the crack equilibrium to be unstable is then given by $dK_*(c)/dc \geqslant dT_0/dc = 0$ in equation (8) or, alternatively, by $dK_A(c)/dc \geqslant dT(c)/dc$ in equation (10) [3]. The latter defines the familiar "tangency" condition for materials with T-curves.

3.2. Microstructural stress intensity factor

Consider the idealised penny crack system in Fig. 4. As discussed in Section 2.1 we suppose that the crack originates within the matrix (i.e. in a region between bridges) subject to the (conservative) tensile stress σ_R, and subsequently spreads into the surrounding regions defined by the (nonconservative) closure stress function $p(u)$. We shall designate contributions to the microstructural toughness term T_μ from the σ_R component by single prime notation, and from the $p(u)$ component by double prime, i.e. $T_\mu = T'_\mu + T''_\mu$. It is convenient to separate the problem into three crack-size regions: c smaller than d (corresponding to first bridge intersections at one half of the spacing 2d in Fig. 1); c larger than d but smaller than the critical size c_* at which the first-intersected bridges just rupture; c larger than c_* (such that the entire bridging zone translates with the advancing tip). As we shall see below (Section 3.2.2), a further subdivision of the second of these regions may be made.

3.2.1. Precursor tensile zone, $c \leqslant d$. Within this region the crack experiences only the matrix tensile stress σ_R. The negative of the stress intensity factor for this region, $T'_\mu = -K'_\mu$, is of the familiar form for uniform stress fields

$$T'_\mu(c) = -\psi\sigma_R c^{1/2} \quad (c \leqslant d) \quad (11)$$

where ψ is a geometry-dependent coefficient appropriate to penny-like cracks. In this region the contribution from $p(u)$ is, of course, zero, i.e.

$$T''_\mu(c) = 0 \quad (c \leqslant d). \quad (12)$$

3.2.2. Bridging zone, $d \leqslant c \leqslant c_*$. Within the bridging zone the crack experiences two contributions, one due to the persistent tensile stresses σ_R over the radial distance $r \leqslant d$ and the other to the frictional closure stresses $p(u)$ over $r \geqslant d$. These microstructural contributions will continue to evolve with crack extension as long as the first-intersected bridge at $r = d$ remains intact.

Start with the first of these contributions, $T'_\mu = -K'_\mu$. We use the Green's function solution for penny-like cracks subject to radially distributed stresses $\sigma(r) = \sigma_R$ over $0 \leqslant r \leqslant d$, $\sigma(r) = 0$ over $r \geqslant d$ ([20])

$$T'_\mu(c) = -(\psi/c^{1/2}) \int_0^d r\sigma(r)\, dr/(c^2 - r^2)^{1/2}$$
$$= -\psi\sigma_R c^{1/2}[1 - (1 - d^2/c^2)^{1/2}]$$
$$(d \leqslant c \leqslant c_*). \quad (13)$$

The following limits are of interest: at $c = d$, $T'_\mu = -\psi\sigma_R d^{1/2}$, as required to match equation (11); at $c \gg d$, $T'_\mu \to -\psi\sigma_R d^2/2c^{3/2}$, which is the solution for a central point-force opening configuration. It is apparent that the influence of the persistent matrix stress diminishes rapidly once the crack enters this bridging zone.

Now consider the second contribution, $T''_\mu = -K''_\mu$. In its exact form, this contribution is expressible as a nonlinear integral equation, which has no general closed-form solution [21]. To avoid a detailed numerical analysis we compute this term analytically in the approximation of "weak shielding" [9, 17], where the influence of the closure stresses is taken into account in the stress intensity factor balance but is ignored in the crack-opening displacement relation. The assumption of weak shielding is appropriate for ceramics with modest toughening characteristics, i.e.

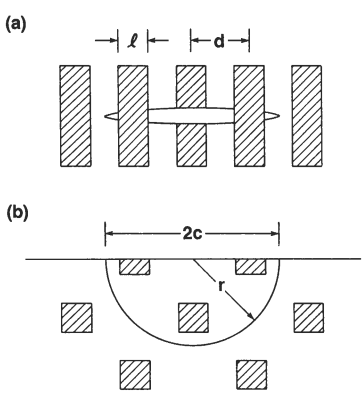

Fig. 4. Growth of penny-like crack in bridging field; (a) side view, (b) projection view. Crack experiences only matrix tensile stresses up to first intersection with bridges at $c = d$. Thereafter, internal stresses rapidly average out to zero across crack plane, and frictional closure forces dominate.

ceramics for which $T''_\mu < T_0$; for our model material this condition is satisfied in the crucial small-crack region (see Section 4, Fig. 7). In this approximation we have [9, 17]

$$T''_\mu(u) = +(E'/T_0)\int_0^{u_Z} p(u)\,du \qquad (14)$$

where u_Z is the crack-opening displacement at the stationary edge of the closure zone, Z in Fig. 5.

The integral in equation (14) is most conveniently taken in two parts, according to whether the crack-opening displacement u is less or greater than u_+ in Fig. 3. For the first region we insert $p(u)$ from equation 5(a)

$$\begin{aligned} T''_\mu(u) &= +(E'/T_0)\int_0^{u_Z} [p_D(u/u_*)^{1/2} - \sigma_R]\,du \\ &= -(E'/T_0)\sigma_R u_Z[1 - (2p_D/3\sigma_R) \\ &\quad \times (u_Z/u_*)^{1/2} \qquad (0 \leqslant u_Z \leqslant u_+). \end{aligned} \qquad (15a)$$

For the second region we insert $p(u)$ from equations 5(a) and (b)

$$\begin{aligned} T''_\mu(u) &= +(E'/T_0)\left\{\int_0^{u_+} [p_D(u/u_*)^{1/2} - \sigma_R]\,du \right. \\ &\quad \left. + \int_{u_+}^{u_Z} [p_M(1 - u/u_*)]\,du\right\} \\ &= (E'/T_0)\{-\sigma_R u_+[1 - (2p_D/3\sigma_R)\,(u_+/u_*)^{1/2}] \\ &\quad + p_M u_*[(u_Z - u_+)/u_*] \\ &\quad \times \{1 - [(u_Z + u_+)/2u_*]\}\} \\ &\quad (u_+ \leqslant u_Z \leqslant u_*). \end{aligned} \qquad (15b)$$

To transform $T_\mu(u)$ to $T_\mu(c)$ we must determine the zone-edge displacement $u_Z = u_Z(c)$ from an appropriate relation for the crack profile. In the spirit of the weak-shielding approximation we use Sneddon's solution for the near-field profile $u(r, c)$ of a crack *free* of microstructural closure terms, but with these same terms *included* implicitly in the equilibrium requirement [$K_* = T_0$ in equation (8)] [8, 9]

$$u(r, c) = (\psi T_0/E'c^{1/2})(c^2 - r^2)^{1/2}. \qquad (16)$$

Then the requisite crack-opening displacement $u = u_Z = u(d, c) = u(c)$ at the zone boundary $r = d$ is

$$u_Z(c) = (\psi T_0/E'c^{1/2})(c^2 - d^2)^{1/2} \quad (d \leqslant c \leqslant c_*). \qquad (17)$$

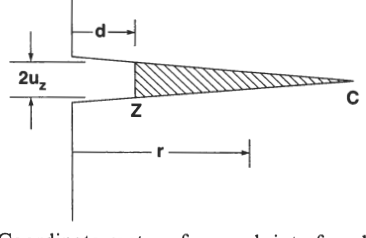

Fig. 5. Coordinate system for crack-interface bridging. C denotes crack tip, Z the edge of the bridging zone at $c = d$.

At the debonding/pullout crossover point $u_Z(d, c_+) = u_+(c) = u_+$ and critical pullout point $u_Z(d, c_*) = u_*(c) = u_*$, equation (17) reduces to

$$u_+ = (\psi T_0/E'c_+^{1/2}) \quad (c_+^2 - d^2)^{1/2} \qquad (18a)$$

$$u_* \simeq \psi T_0 c_*^{1/2}/E' \quad (c_* \gg d) \qquad (18b)$$

respectively, where c_+ and c_* define the corresponding crack sizes.

3.2.3. Steady-state zone, $c \geqslant c_*$. Once the critical first-intersected bridge at Z (Fig. 5) is ruptured the entire bridging zone translates with the advancing crack tip. In the limit $c_* \gg d$, equation (13) becomes

$$T'_\mu = 0. \qquad (19)$$

For $u_* \gg u_+$, $c_* \gg c_+$, evaluation of equation (15b) at $u_Z = u_*$ similarly gives

$$T''_\mu \simeq +E'p_M u_*/2T_0 \quad (u \geqslant u_*). \qquad (20)$$

3.3. T-curve

We now have all the ingredients for constructing the T-curve. At this stage it is convenient to introduce some coefficients that characterise the geometrical features of the microstructure in relation to the grain size, l (Fig. 1). This introduces the concept of *geometrical similitude*: for microstructures that change only in *scale* and not in the essential geometry such coefficients remain invariant. Thus we define the following similitude constants

$$\alpha_d = d/l \qquad (21a)$$

$$\alpha_L = L/l \qquad (21b)$$

$$\alpha_\lambda = \lambda/l \qquad (21c)$$

$$\epsilon_L = 2u_*/L. \qquad (21d)$$

The coefficient α_d relates the bridge spacing to the grain size (unity for equiaxed microstructures, Section 2.1), and generally defines the area fraction of bridges $(1/2\alpha_d^2)$; α_L is the aspect ratio of the pullout grains, with L the long (embedded) dimension (again, unity for equiaxed microstructures); α_λ is the cross-sectional perimeter to grain-diameter ratio for the embedded grain (4 for grains of rectangular cross section); and ϵ_L is the "bridge rupture strain". Then we may substitute into equations (7) and (11–20) to determine $T(c) = T_0 + T'_\mu(c) + T''_\mu(c)$ in the following crack-size regions

$$T(c) = T_0 - \psi\sigma_R c^{1/2} \quad (c \leqslant \alpha_d l) \qquad (22a)$$

$$\begin{aligned} T(c) &= T_0 - \psi\sigma_R c^{1/2}\{1 - (2p_D/3\sigma_R)(c/c_*)^{1/4} \\ &\quad \times (1 - \alpha_d^2 l^2/c^2)^{3/4} \quad (\alpha_d l \leqslant c \leqslant c_+) \end{aligned} \qquad (22b)$$

$$\begin{aligned} T(c) &= T_0 - \psi\sigma_R c^{1/2}\{1 - (1 - \alpha_d^2 l^2/c^2)^{1/2} \\ &\quad + (c_+/c)^{1/2}\,(1 - \alpha_d^2 l^2/c_+^2)^{1/2}[1 - (2p_D/3\sigma_R) \\ &\quad \times (c_+/c_*)^{1/4}(1 - \alpha_d^2 l^2/c_+^2)^{1/4}]\} \\ &\quad + \psi p_M c^{1/2}\{(1 - \alpha_d^2 l^2/c^2)^{1/2} - (c_+/c)^{1/2} \\ &\quad \times (1 - \alpha_d^2 l^2/c_+^2)^{1/2}\}\,\{1 - \tfrac{1}{2}[(c/c_*)^{1/2} \end{aligned}$$

$$\times (1 - \alpha_d^2 l^2/c^2)^{1/2} + (c_+/c_*)^{1/2}$$

$$\times (1 - \alpha_d^2 l^2/c_+^2)^{1/2}]\} \quad (c_+ \leqslant c \leqslant c_*) \tag{22c}$$

$$T(c) = T_0 + \tfrac{1}{2}\psi p_M c_*^{1/2} = T_\infty \quad (c \geqslant c_*) \tag{22d}$$

with

$$p_D = (\alpha_\lambda \epsilon_L \alpha_L \mu \sigma_R E)^{1/2}/(2\alpha_d^2 - 1) \tag{23a}$$

$$p_M = \alpha_\lambda \epsilon_L \alpha_L \mu \sigma_R (1 - 1/2\alpha_d^2) \tag{23b}$$

$$c_* \simeq (\epsilon_L \alpha_L E' l/2\psi T_0)^2 \tag{23c}$$

$$[(c_+^2 - \alpha_d^2 l^2)/c_+]^{1/2} = (\epsilon_L \alpha_L E' l/2\psi T_0)$$

$$\times (p_D/2p_M)^2 \{[1 + 4p_M$$

$$\times (p_M + \sigma_R)/p_D^2]^{1/2} - 1\}^2 \tag{23d}$$

the last (implicit) equation defining c_+. Note it is only the spatial scaling terms c_* and c_+, and not the stress scaling terms p_D and p_M, that depend on l. Evaluation of equation (22) indicates that $T(c)$ drops *below* T_0 in its initial extension within $c \leqslant d$, but quickly increases above T_0 once the bridging zone is entered and the crack extends beyond c_+, ultimately saturating at its steady state value for $c \geqslant c_*$. We shall illustrate this general trend for our model alumina material in Section 4 below.

3.4. Strength characteristics for indentation flaws

Consider finally the conditions for Vickers half-penny indentation cracks produced at load P to proceed to unlimited failure under the action of an applied tensile stress σ_a. From those conditions we may compute the *inert strength* σ_m (i.e. the strength in the absence of any kinetic effects) as a function of P, and thence establish the basis for deconvolution of the T-curve from experimental data.

Begin by writing $K_A(c)$ in equation (10) in the familiar form for such cracks

$$K_A(c) = \psi \sigma_a c^{1/2} + \chi P/c^{3/2} \tag{24}$$

where χ is a coefficient denoting the intensity of the residual Vickers elastic–plastic contact deformation field [22–24]. At equilibrium, $K_A(c) = T(c)$, we have

$$\sigma_a(c) = (1/\psi c^{1/2})[T(c) - \chi P/c^{3/2}]. \tag{25}$$

We now seek an instability condition for $\sigma_a(c)$. Recall from Section 3.1 that the requirement for instability is $dK_A(c)/dc \geqslant dT(c)/dc$. In terms of equation (25) this condition is equivalent to $d\sigma_a(c)/dc \geqslant 0$ [13]. In general (as we shall demonstrate in Section 4), $\sigma_a(c)$ has two maxima, one on either side of $c = d$: that at $c < d$ is governed by the shorter-range influence of the residual contact field (K_r); that at $c > d$ is governed by the longer-range influence of the microstructural interaction ($K_\mu = -T_\mu$) [9]. The relative heights of the two barriers is determined by the indentation load. Once the first barrier (at $c < d$) is surmounted the crack becomes unstable. However, the crack propagates spontaneously to failure only if the second barrier (at $c > d$) is lower. If the second barrier is higher the crack will arrest on a stable branch of the $\sigma_a(c)$ curve ("pop in") before an unlimited instability can be achieved. Thus the *strength* σ_m is determined by the greater of the two maxima.

It remains to demonstrate how one may solve equation (25) numerically for the strength characteristic, and thence extract the $T(c)$ curve, for a given material system.

4. CASE STUDY ON AN ALUMINA CERAMIC

We demonstrate the above fracture mechanics formalism by analysing indentation-strength, $\sigma_m(P)$, data for a particular polycrystalline alumina ceramic.† This alumina, apart from exhibiting significant T-curve characteristics, has served as a model material in previous studies of the bridging mechanism [3, 4, 7]. It is a *nominally* pure material with grain size $l \approx 20\ \mu$m. In actuality, the material contains a small amount of sintering aid (<0.1% MgO and other oxide additive) and has a noticeably nonuniform, nonequiaxed grain distribution (e.g. see micrographs in Ref. [7]), but we shall regard these as mere "perturbations" of an otherwise regular microstructure.

The analytical procedure involves selecting the parameters in equations (21), (22) and (25) to get an iterative best fit to the $\sigma_m(P)$ data. It is similar in principle to the procedure described in an earlier study [9], but with some refinements.

4.1. Fitting procedure

The first step is to specify initial values for the T-curve parameters:

(*i*) *Material parameters.* First we specify Young's modulus E and Vickers hardness H for our alumina. The values $E = 393$ GPa (Poisson's ratio $\nu = 0.20$) and hardness $H = 19.1$ GPa are taken from earlier data [9]. These values are sufficiently accurate ($< \pm 1\%$ uncertainty) as to be treated as invariants in the iteration process.

The intrinsic grain boundary toughness T_0 and internal stress σ_R can not be specified to the same degree of accuracy (probably not much better than $\pm 30\%$). For T_0 we write $T_0/T_S = (1 - \gamma_B/2\gamma_S)^{1/2}$ from equations (8) and (9), with $T_S = 3.1\ \text{MPa}\cdot\text{m}^{1/2}$ the toughness of single crystal sapphire [9]: using a most recent estimate $\gamma_B/\gamma_S = 1.05$ (median) from dihedral angle measurements of thermal grooves at grain-boundary/free-surface junctions in MgO-doped alumina polycrystals [25], we obtain $T_0 = 2.1\ \text{MPa}\cdot\text{m}^{1/2}$; however, an earlier estimate $\gamma_B/\gamma_S = 0.54$ in bicrystals [26] suggests that the true value of T_0 could be somewhat larger. For σ_R we take a value 100 MPa (mean) from measurements of the broadening of

†Vistal grade Al_2O_3, Coors Ceramics Co., Golden, Colorado.

spectroscopic lines [27]. In view of the abovementioned uncertainty level, T_0 and σ_R are regarded as subject to minor adjustment.

(*ii*) *Bridging parameters.* The bridge rupture strain ϵ_L and the sliding friction coefficient μ are even more difficult to specify *a priori*. An esimate of ϵ_L may be obtained directly from microscopic measurements of crack-opening displacements. For our alumina grain size $l = 20\ \mu$m, displacements $u_* = 1$–$2\ \mu$m have been observed at active bridging sites some millimeters behind the crack tip, corresponding to $\epsilon_L \approx 0.05$–0.10 (e.g from micrographs in Ref. [7]). Reichl and Steinbrech [28], in a more detailed study of several "pure" aluminas in the grain size range 3–17 μm, found $\epsilon_L \simeq 0.12$. This parameter probably depends strongly on the detailed grain geometry, so again we regard it as an adjustable, with $\epsilon_L \approx 0.10$ as our starting value.

As with any dissipative quantity, the friction coefficient μ is notoriously difficult to predetermine for any given material system. We have already alluded to the existence of geometrical irregularities that might augment μ in the grain pullout configuration (Section 2.3), suggesting that we should not be surprised to find unusually large values. A starting estimate of this parameter is accordingly obtained by trial and error using the algorithm described below (Section 4.2) in preliminary data-fit runs.

(*iii*) *Flaw parameters.* Next, we specify the parameters that characterise the Vickers indentation flaws. We use "calibrated" values from previous indentation studies [9]: the geometrical constant $\psi = 1.24$ (close to value 1.27 for ideal penny cracks), and the residual-contact-intensity coefficient $\chi = 4.0 \times 10^{-3}\ (E/H)^{1/2}$. These are taken as invariants.

(*iv*) *Similitude parameters.* Lastly, we specify the α similitude parameters in equation (21). We take $\alpha_d = 1 = \alpha_L$ and $\alpha_\lambda = 4$, corresponding to an ideally

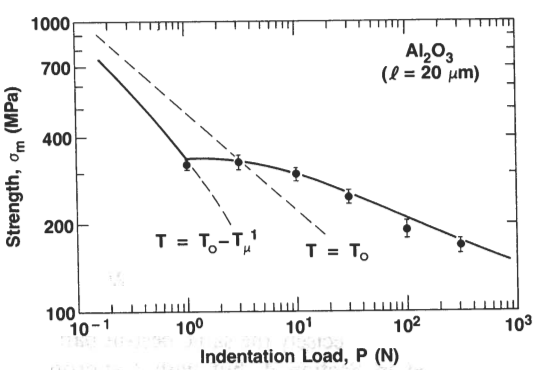

Fig. 6. Plot of $\sigma_m(P)$ for selected alumina material of grain size $l = 20\ \mu$m. Points with standard deviation error bars are experimental data from reference [3]. Solid curve is best fit of bridging theory to these points. Dashed curve at extreme left is corresponding hypothetical curve for same material with matrix tensile stresses present but with no bridging tractions ($T = T_0 - T'_\mu$); central dashed curve corresponds to same material but with no bridging *or* internal stresses ($T = T_0$).

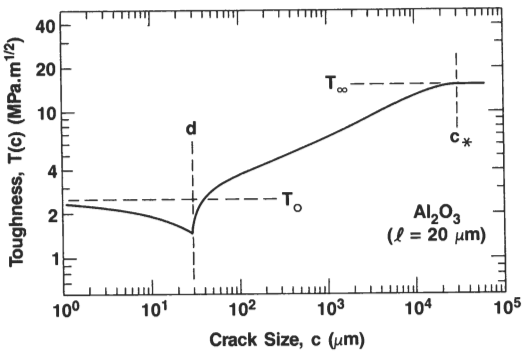

Fig. 7. Deconvoluted toughness $T(c)$ function, equation (22), for selected alumina, corresponding to data fit in Fig. 6. The falloff in the function below T_0 prior to first bridge intersection at $c = d$ is indicative of the initially deleterious effect of (tensile) matrix internal stresses. Thereafter the crack becomes dominated by the beneficial influence of frictional grain pullout tractions, whence the curve rises above T_0 again to its saturation value T_∞ at $c = c_*$.

equiaxed and rectangular microstructure. We regard α_L and α_λ as invariants, noting from equation (23) that errors in these terms can be largely accommodated in the adjustments of ϵ_L and μ. The bridge spacing parameter α_d we allow to vary.

We then use the following regression algorithm for best-fitting the $\sigma_m(P)$ data:

(i) After evaluating the scaling stress (p_D, p_M) and spatial (c_*, c_+) terms in equation (23) using the starting parameters from Section 4.1, compute a trial T-curve from equation (22).

(ii) Compute the function $\sigma_a(c)$ in equation (25) for each indentation load P for which experimental data are available. Determine the strength σ_m as the maximum in this function at each of these loads (recalling that if two maxima exist it is the greater which determines σ_m).

(iii) Compare computed strengths with measured values, and thence evaluate the residual,

$$\sum_n [\sigma_m(P)_{calc} - \sigma_m(P)_{meas}]^2/(n-1),$$

over all n loads.

(iv) Increment the adjustables ϵ_L and μ in a "coarse" first-run matrix search routine (in steps 10% of starting values), and cycle (i)–(iii). Invoke a minimum variance condition to determine interim best-fit values.

(v) Increment the adjustables ϵ_L, μ, T_0, σ_R and α_d in a "fine", second-run routine (ultimately, in steps of 1% of starting value), and proceed similarly to determine final best-fit values.

4.2. Results

The results of the data analysis for our model alumina are summarised in Figs 6–8, corresponding to final best-fit values $\epsilon_L = 0.135$, $\mu = 1.80$, $T_0 = 2.50\ \text{MPa}\cdot\text{m}^{1/2}$, $\sigma_R = 155\ \text{MPa}$ and $\alpha_d = 1.50$.

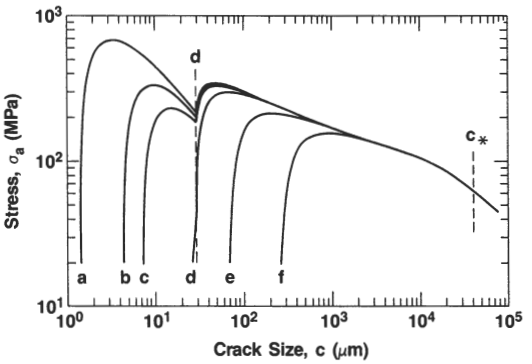

Fig. 8. Plots of $\sigma_a(c)$, equation (25), for selected alumina, using the parametric determinations from Figs 6 and 7. Curves are for indentation loads P covering the data range in Fig. 6: (a) 0.2 N; (b) 1 N; (c) 2 N; (d) 10 N; (e) 100 N; (f) 1000 N.

We note that ϵ_L corresponds to the Reichl and Steinbrech value quoted above; that μ is substantial, as foreshadowed in Section 2.3; that the values of T_0 and σ_R are not substantially different from the first, trial estimates; and that α_d corresponds to a bridge at every third grain. In Fig. 6 the solid curve represents the fit to the experimental $\sigma_m(P)$ data points (error bars on the data points representing standard deviations) [3]. The theory accounts for the major trends in the data, in particular the tendency to a plateau strength at diminishing indentation loads (shorter initial crack lengths).

Also plotted in Fig. 6, as the two dashed curves at left, are the predicted responses for the same alumina corresponding to the following hypothetical "toughness states": frictional stresses "switched off", i.e. bridges removed ($p_D = 0 = p_M$, $d = \infty$), but matrix internal stresses ever present ($\sigma_R \neq 0$), $T = T_0 - T'_\mu$; frictional *and* internal stresses switched off ($p_D = 0 = p_M$, $d = \infty$, $\sigma_R = 0$), $T = T_0$. These two curves quantify the degrading effect of the internal stress on the strength at low indentation loads (small flaw sizes); and, conversely, the (over-) compensating effect of the friction at high loads (large flaw sizes), leading ultimately to the macroscopic toughness state $T = T_\infty$.

The deconvoluted T-curve corresponding to the data fit is shown in Fig. 7. The previously mentioned tendency for $T(c)$ to drop below T_0 prior to intersecting the first bridges at $c = d$ (section 3.3) is apparent in this diagram. This is a facet of T-curve behaviour that escapes detection in traditional, large-scale crack tests, where the initial stages of crack propagation generally occur from ill-defined, rounded notches. The fall-off in $T(c)$ continues in the immediate aftermath of the first bridge intersection as the crack enters the debonding zone $d \leqslant c \leqslant c_+$, although in our material this region is so small ($c_+/d \leqslant 1.01$) as to be undetectable in Fig. 7. Once the crack enters the frictional sliding zone $c_+ \leqslant c \leqslant c_*$ the T-curve rises rapidly until, at $c \geqslant c_*$, it begins its familiar rise toward saturation at $T = T_\infty$. This plot shows again that the internal stress is an important factor in the toughness characteristic; but that in the frictional contribution it is only the pullout, and not the debonding, that is important.

Figure 8 shows plots of applied stress vs crack size for our alumina at different indentation loads. These plots illustrate the instabilities that occur in the crack evolution to failure. At large P it is the second maximum, i.e. the maximum associated with the bridging, that dominates [9]. Within the plateau strength region of Fig. 6 the initial crack "pops in" before growing stably to failure, consistent with observation [7]. The stabilising effect of the bridging is evident in this region as the relative insensitivity of the second maximum to P. At very small P it is the first maximum, associated with the residual contact field, that dominates. In principle, indentations in this region should allow us to explore the extreme left-hand branch of the $\sigma_m(P)$ plot in Fig. 6, but the almost invariable presence of natural flaws in the size range $c > d$ generally precludes the possibility of exceeding the plateau strength level [3, 9].

5. GRAIN-SIZE DEPENDENCE OF STRENGTH

Let us demonstrate the versatility of the "calibrated" formulation above by considering the grain-size dependence of the T-curve, $T(c)$, and thence the indentation–strength function, $\sigma_m(P)$, for alumina ceramics. There are few systematic experimental studies of such grain-size dependencies in alumina (or, indeed, in any other polycrystalline ceramic material) in the literature. However, there are some earlier indentation–strength data for two aluminas, nominally pure with grain sizes 3 and 25 μm, that we may usefully compare with the results for our reference material in Section 4 [3].† Also, there are some unpublished bend–strength data by Charles and Shaw [29] on as-fired "pure" aluminas with grain sizes in the range 6–150 μm that allow a tentative investigation of the underlying $\sigma_m(l)$ relation for "natural" flaws.

Consider first the indentation–strength data [3] for the 3 and 25 μm aluminas in Fig. 9. We make our comparison by generating the appropriate $\sigma_m(P)$ functions using precisely the same best-fit parameters as obtained in Section 4, but with l appropriately adjusted. These functions are plotted as the solid curves in Fig. 9, along with their counterpart for $l = 20\,\mu$m (dashed line) from Fig. 6. The calibrated theory therefore has the capacity to predict at least qualitative trends in strength and toughness characteristics with change in the important microstructural parameters.

†AD999 grade (3 μm), and heat-treated Vistal grade (25 μm). Coors Ceramics Co., Golden, Colorado.

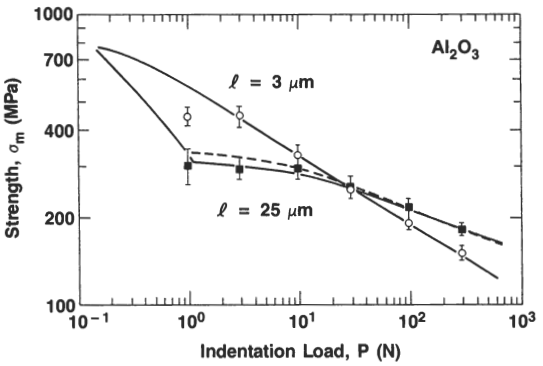

Fig. 9. Plots of $\sigma_m(P)$ for alumina materials of grain size $l = 3$ and 25 μm. Points with standard deviation error bars are experimental data from Ref. [3]. Solid curves are predictions of bridging theory appropriate to these grain sizes, using best-fit parameters from the reference alumina material ($l = 20\,\mu$m) from Fig. 6. [Reference $\sigma_m(P)$ curve included here as dashed curve for comparison.]

The informational value of comparative predictions of the type illustrated in Fig. 9 is manifest in the way the curves cross each other. It becomes clear that there can be no simple, single grain-size dependence of strength for materials with strong T-curves (R-curves). In particular, the familiar $l^{-1/2}$ (Hall–Petch) dependence does not appear to be obeyed in any crack-size region. Thus, whereas the plateau σ_m tends to diminish with increasing l at low loads (small c), the dependence on l is somewhat less strong than $l^{-1/2}$. At high loads (large c), σ_m actually increases with l.

Now consider how the theory compares with the available $\sigma_m(l)$ data [29] for failures from "natural" flaws, Fig. 10. The solid line appropriately represents the predicted dependence of plateau strength for flaws without any residual nucleation field (i.e. $K_r = 0$), once more using the best-fit parameters from the reference alumina material and treating l as an independent variable. We may note that the slope of this line is close to 1/3; and that a force-fitted line with the classical Hall–Petch slope 1/2 cannot be made to pass through the error bars on the data points.

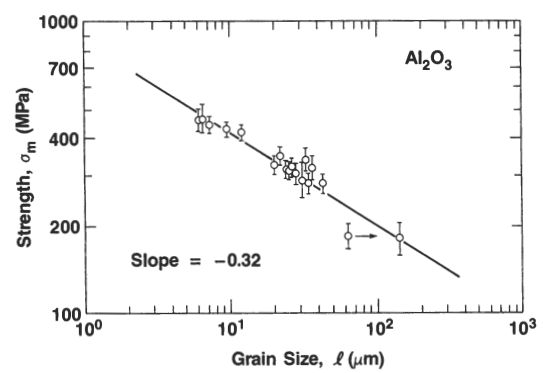

Fig. 10. Strength vs grain size for polycrystalline alumina. Data points from Ref. [29], means and standard deviations of insert bend strengths for specimens with "natural" flaws (as-fired "Lucalox®" specimens). Solid line from bridging theory, predicted plateau strengths for natural flaws, using best-fit parameters from the reference alumina material. (Arrow on data point at $l = 66\,\mu$m indicates a material with exceptionally broad grain size distribution [29].)

6. DISCUSSION

Our toughness/crack-size (T-curve, or R-curve) model is based on a physical microstructural constitutive relation for crack interfacial bridging, in which thermal expansion mismatch stresses are a governing factor in determining dissipative Coulomb frictional pullout tractions at interlocking grains. The model accounts for the major features of the T-curve function, notably the magnitude and range, for nontransforming ceramics. We emphasise, however, that our $T(c)$ functions have had to be best-fitted to the experimental (indentation-strength) data, with adjustable parameters. In addition, the formulation embodies several approximations, e.g. weak-shielding, undistorted Sneddon crack profile, negligible transgranular fracture. Furthermore, we have given explicit consideration here to just one ceramic material, alumina. Accordingly, any "goodness of fit" evident in the analysis of Sections 4 and 5 is not to be construed as proving the general validity of the bridging model. Such proof comes from independent, *in situ* observation of crack micromechanics on this alumina [7] as well as on a wide range of other nontransforming ceramics [10], not from conventional macroscopic fracture mechanics measurements. However, the fit does confirm that the bridging model can account for most documented characteristics of T-curve (R-curve) behaviour, e.g. the flaw tolerance quality and grain-size dependencies.

Moreover, once the $T(c)$ function has been "calibrated" against a "reference" data set, as in Section 3, we have the power to predict how the T-curve and associated $\sigma_m(P)$ functions should vary with changes in the microstructure. We alluded to this power in our brief consideration of the strength/grain-size dependence for alumina ceramics in Section 4. A more detailed study of the $\sigma_m(l)$ dependence in aluminas is currently under way [30]. Similar dependencies of strength on grain boundary toughness (T_0), internal stress level (σ_R), grain–grain friction coefficient (μ), may be similarly evaluated. These are additional factors that might be systematically adjusted by material processors to improve strength characteristics. Thus we have a physically sound basis for optimising the microstructures of the broad range of structural ceramic materials whose toughness behaviour is governed by the bridging mechanism.

The *a priori* specification of a constitutive stress-separation law is manifestly the single most important factor that distinguishes the present analysis from previous treatments [8, 9]. The inclusion of the internal stress parameter σ_R is an especially unique

feature. Its strong influence on the mechanical response is apparent in Figs 6 and 7: in Fig. 6 as the comparison between solid $\sigma_m(P)$ curve (data fit for fully bridged crack) and central dashed curve (zero internal stress, zero bridging), indicative of a countervailing lowering and raising of the strength at small and large crack sizes respectively; in Fig. 7 correspondingly as the initially falling ($c < d$) but ultimately rising $T(c)$ curve ($c \gg d$). We see that the influence of σ_R can be deleterious at small c, but that this deleterious influence may be more than compensated, via the dissipative frictional sliding interaction, at large c. The route to flaw tolerance is therefore a delicate one of balancing positive and negative elements of inbuilt stress states at opposite ends of the flaw-size spectrum.

It is useful to pursue the issue of short cracks vs long cracks in the context of traditional fracture mechanics testing. Some recent experimental results reported by Steinbrech and Schmenkel [12] on a nominally pure alumina of grain size $l = 13\,\mu$m are especially well suited for this purpose. Those authors measured crack growth from single-edge-notched beam specimens to obtain $T(c)$ data on the macroscopic scale, and from naturally occurring flaws in four-point-bend specimens to obtain comparative data on the microscopic scale. Their results are plotted in Fig. 11, together with the theoretically predicted curve for the appropriate grain size from our "calibrated" equation (22). The theoretical curve appears at least to reflect the broader trends of the rising $T(c)$ curve at large c, although we can hardly expect any such extrapolation of the indentation-strength-calibrated curve to provide an accurate representation in this long-crack domain. Conversely, it is evident that there are important features of the $T(c)$ function at small c which may not be readily quantified by experimentation with long-crack specimens. In particular, the fall-off in $T(c)$ at $c < d$ associated with internal tensile matrix stresses will generally pass unnoticed in such specimens. This is the domain of short cracks, where microstructure-scale instabilities in the initial growth (e.g. the initial "pop-in" referred to in Section 4) can occur.

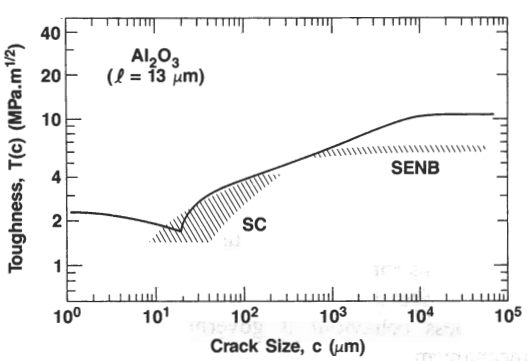

Fig. 11. Comparison of $T(c)$ data obtained by Steinbrech & Schmenkel [12] (shaded areas) on a nominally pure alumina of grain size $l = 13\,\mu$m using surface cracks (SC) in four-point bend and single-edge-notched-beam (SENB) and specimens with small-scale flaws with theoretically-predicted curve from present analysis.

If this last point concerning short-crack instabilities is not readily apparent in conventional crack-growth tests, it certainly is manifest in one well-documented aspect of the fracture behaviour of ceramics. This is the tendency of those ceramics with large internal stresses to exhibit spontaneous microfracture at some critical grain size. Let us note that the shape of the diminishing $T(c)$ curve in Fig. 7 prior to the first bridge intersection at $c = d$ is independent of grain size l [equation (22a)]. The effect of increasing d will thus be to extend this portion of the $T(c)$ curve further downward. If we were to scale up l such that $T(c)$ were to intersect the c-axis before the condition $c = d$ is satisfied, then pre-existing flaws would become amenable to unstable extension without any external load applied. Hence the phenomenon of spontaneous microfracture may be seen as a natural, limiting consequence of our model.

The implications of the bridging mechanics presented here extend beyond the immediate question of inert strength, to fatigue and lifetime analysis [31] and to wear properties of brittle ceramics [32].

Acknowledgements—The authors gratefully acknowledge many fruitful discussions with D. B. Marshall, R. F. Cook, Y-W. Mai and S. Lathabai. Funding was provided by the U.S. Air Force Office of Scientific Research.

REFERENCES

1. H. Hubner and W. Jillek, *J. Mater. Sci.* **12,** 117, (1977).
2. R. W. Steinbrech, R. Knehans and W. Schaarwachter, *J. Mater. Sci.* **18,** 265 (1983).
3. R. F. Cook, B. R. Lawn and C. J. Fairbanks, *J. Am. Ceram. Soc.* **68,** 604 (1985).
4. C. J. Fairbanks, B. R. Lawn, R. F. Cook and Y-W. Mai, *Fracture Mechanics of Ceramics* (edited by R. C. Bradt, A. G. Evans, D. P. H. Hasselman and F. F. Lange), Vol. 8, p. 23. Plenum, New York (1986).
5. F. Duerler, R. Knehans and R. W. Steinbrech, *J. Physique* **C1,** 617 (1986).
6. H. Wieninger, K. Kromp and R. F. Pabst, *J. Mater. Sci.* **21,** 411 (1986).
7. P. L. Swanson, C. J. Fairbanks, B. R. Lawn, Y-W. Mai and B. J. Hockey, *J. Am. Ceram. Soc.* **70,** 279 (1987).
8. Y-W. Mai and B. R. Lawn, *J. Am. Ceram. Soc.* **70,** 289 (1987).
9. R. F. Cook, C. J. Fairbanks, B. R. Lawn and Y-W. Mai, *J. Mater. Res.* **2,** 345 (1987).
10. P. L. Swanson, *Advances in Ceramics*, Vol. 22, p. 135. Am. Ceram. Soc., Columbus, Ohio (1988).
11. Y-W. Mai, *Mater. Forum* **11,** 232 (1988).
12. R. W. Steinbrech and O. Schmenkel, *J. Am. Ceram. Soc.* **71,** C-271 (1988).
13. Y-W. Mai and B. R. Lawn, *Ann. Rev. Mater. Sci.* **16,** 415 (1986).
14. R. Ballarini, S. P. Shah and L. M. Keer, *Engng Fract. Mech.* **20,** 433 (1984).
15. R. W. Rice, R. C. Pohanka and W. M. McDonough, *J. Am. Ceram. Soc.* **63,** 703 (1980).
16. M. V. Swain, *J. Mater. Sci.* **5,** 1313 (1986).
17. D. B. Marshall and A. G. Evans, *Mater. Forum* **11,** 304 (1988).

18. A. G. Evans, A. H. Heuer and D. L. Porter, *Fracture 1977* (edited by D. M. R. Taplin), Vol. 1, p. 529. Univ. of Waterloo Press, Waterloo (1977).
19. B. R. Lawn and T. R. Wilshaw, *Fracture of Brittle Solids*, Chap. 2. Cambridge Univ. Press (1975).
20. H. Tada, P. C. Paris and G. R. Irwin, *Stress Analysis of Cracks Handbook*. Paris Productions, St Louis, Mo. (1985).
21. J. R. Rice, *Treatise on Fracture* (edited by H. Liebowitz), Vol. II, Chap. 3. Academic Press, New York (1968).
22. D. B. Marshall and B. R. Lawn, *J. Mater. Sci.* **14,** 2001 (1979).
23. D. B. Marshall, B. R. Lawn and P. Chantikul, *J. Mater. Sci.* **14,** 2225 (1979).
24. B. R. Lawn, A. G. Evans and D. B. Marshall, *J. Am. Ceram. Soc.* **63,** 574 (1980).
25. C. A. Handwerker, J. M. Dynys, R. M. Cannon and R. L. Coble, *J. Am. Ceram. Soc.* In press.
26. J. F. Shackelford and W. D. Scott, *J. Am. Ceram. Soc.* **51,** 688 (1968).
27. J. E. Blendell and R. L. Coble, *J. Am. Ceram. Soc.* **65,** 174 (1982).
28. A. Reichl and R. W. Steinbrech, *J. Am. Ceram.* **71,** C-299 (1988).
29. R. J. Charles and R. R. Shaw, General Electric Report No. 62-RL-3081M.
30. P. Chantikul, S. J. Bennison and B. R. Lawn. In preparation.
31. S. Lathabai and B. R. Lawn, *J. Mater. Sci.* In press.
32. S. J. Cho, B. J. Hockey, B. R. Lawn and S. J. Bennison, *J. Am. Ceram. Soc.* In press.

APPENDIX

Calculation of Frictional Debonding Stress–Separation Function

In this Appendix we reproduce the essence of a calculation by Marshall and Evans [17] for frictional debonding. We assume that debonding begins at the crack plane and works itself up the matrix–grain interface a distance Y as the crack walls separate through displacement u, Fig. 2. At first, we suppose only that shear-lag tractions $\tau(y)$ do exist, and only later connect these tractions with internal stresses.

Consider an elemental area of matrix–grain interface bounded by y and $y + \mathrm{d}y$. At equilibrium, the frictional traction τ over this area must be balanced by the axial internal stress $\sigma(y)$ in the embedded grain, i.e. $l^2\,\mathrm{d}\sigma(y) = -\tau\lambda\,\mathrm{d}y$, or

$$\mathrm{d}\sigma/\mathrm{d}y = -\tau\lambda/l^2. \tag{A1}$$

This equation may be integrated at constant τ (neglecting any elastic stresses at $y > Y$), over $y = 0$ to $y = Y$. We take as boundary conditions $\sigma(0) = p_0(l^2/2d^2)$ [recall from equation (2) that $l^2/2d^2$ is area fraction of bridges] and $\sigma(Y) = p_0$, where p_0 is the stress exerted by the embedded grain in the absence of any residual stresses. The integration gives

$$p_0 = (\tau\lambda Y/l^2)/(2d^2/l^2 - 1). \tag{A2}$$

The strain in the grain (measured relative to the strain endured if sliding were to be prevented [17]) at the debond length Y is

$$u/Y = \tfrac{1}{2}(p_0/E)(2d^2/l^2 - 1) \tag{A3}$$

where the factor two is because the strain has a linear gradient along y. Eliminating Y from equations (A2) and (A3) gives

$$p_0(u) = (2\tau E\lambda u/l^2)^{1/2}/(2d^2/l^2 - 1). \tag{A4}$$

Now suppose that the friction is Coulombic, i.e. due to residual internal stresses. Then we may write immediately, $\tau = \mu\sigma_{\mathrm{R}}^{-}$. In addition, we must replace p_0 by $p_0 + \sigma_{\mathrm{R}}$, to allow for the residual opening force exerted by the embedded grain on the matrix at zero crack-wall displacement [17]. With equation (2), these modifications lead to our final constitutive relation for debonding

$$p(u) = [(2\mu\sigma_{\mathrm{R}} E\lambda/l^2)^{1/2}/(2d^2/l^2 - 1)]u^{1/2} - \sigma_{\mathrm{R}} \tag{A5}$$

as per equation (3) in the text.